



# Molecular dynamics study on phase change properties and their nano-mechanism of sugar alcohols: Melting and latent heat

Shukai Cheng<sup>a,b,\*</sup>, Donatas Surblis<sup>b</sup>, Taku Ohara<sup>b</sup>

<sup>a</sup> Department of Finemechanics, Graduate School of Engineering, Tohoku University, Sendai, 980-8579, Japan

<sup>b</sup> Institute of Fluid Science, Tohoku University, Sendai, 980-8577, Japan

## ARTICLE INFO

### Keywords:

Molecular dynamics  
Phase change materials  
Sugar alcohols  
Melting  
Latent heat

## ABSTRACT

Sugar alcohol phase change materials have gained considerable attention for heat storage in recent years owing to their higher thermal conductivity and larger latent heat compared to traditional paraffin materials. However, knowledge about the reason of large latent heat and latent heat difference among diverse sugar alcohols as well as the mechanism of melting process remains elusive. In this study, molecular dynamics simulation was employed to investigate the melting process and latent heat of four sugar alcohols (glycerol, erythritol, arabinitol, and mannitol). Melting points and latent heat of fusion were determined first, different melting temperatures were observed under different one-dimensional heat conduction directions in several sugar alcohols. It was found that the strength of intermolecular interactions within molecular crystal layers has a positive correlation with the anisotropic melting tendencies, which can be more intuitively reflected by the difference in the number of hydrogen bonds within the molecular layers. In addition, the decomposition of the latent heat of fusion revealed that the latent heat is mainly composed of van der Waals and Coulombic contributions, where the interaction between hydroxyl groups accounts for a major part. Hydrogen bond analysis demonstrated that the latent heat of fusion is partly due to the breakage of hydrogen bonds during the phase transition of melting. It was also noted that the differences in the hydrogen bonding lifetimes between different sugar alcohols may be related to the magnitude of latent heat of fusion. Erythritol and mannitol which coincidentally happened to have an even number of carbon atoms can fulfill the properties of better PCMs compared to glycerol and arabinitol, which have an odd number of carbons. Those results will pave the way for better design optimization and performance evaluation of sugar alcohols as phase change materials.

## 1. Introduction

With the development of technology and the progress of society, energy utilization is increasing rapidly. The process of energy extraction and use is inevitably accompanied by waste and pollution of the environment due to its byproducts. Therefore, energy depletion and environmental degradation are imminent problems that human society must face and address. In order to better enhance the utilization efficiency of energy as well as reduce waste, phase change materials (PCMs) emerged as a new approach to thermal energy storage [1]. PCMs can undergo a phase change at a certain condition and absorb or release a large amount of energy during the phase change process, which is mostly helped by latent heat. Due to this, PCMs are used in a wide range of applications in the construction, refrigeration, and energy sectors [2,3]. Specifically, the large latent heat of sugar alcohol PCMs has drawn much attention

from researchers and industry.

Generally, PCMs are categorized into organic and inorganic [4]. Many experimental works show that organic PCMs have better recyclability, weaker aggregation, and melting temperatures that are in the range working temperatures of most thermal management systems, which make them a more attractive choice for research and real-life applications [5]. When considering phase change types, they can be divided into liquid-gas, solid-solid, and solid-liquid PCMs, among which, solid-liquid PCMs are of greatest interest because of their small volume change during melting or solidification, and their high latent heat (latent heat of fusion) [6]. Among such solid-liquid PCMs, paraffin wax is a convenient and inexpensive organic PCM that has been widely investigated by researchers via both experiments and simulations. On the other hand, paraffin wax PCMs have low thermal conductivity which prevents the stored heat from being emitted in a timely manner and leads to poor

\* Corresponding author.

E-mail address: [cheng.shukai.p8@dc.tohoku.ac.jp](mailto:cheng.shukai.p8@dc.tohoku.ac.jp) (S. Cheng).

<https://doi.org/10.1016/j.ijheatmasstransfer.2024.126104>

Received 6 May 2024; Received in revised form 11 July 2024; Accepted 19 August 2024

Available online 27 August 2024

0017-9310/© 2024 The Authors. Published by Elsevier Ltd. This is an open access article under the CC BY license (<http://creativecommons.org/licenses/by/4.0/>).

efficiency during applications requiring fast exchange of heat, motivating further search for improvements [7]. Approaches including introducing high thermal conductivity materials, nano-encapsulation, and functional group modification have been applied to improve the thermal conductivity of paraffin PCMs. Unfortunately, this enhancement is usually accompanied by latent heat attenuation [8,9].

In recent years, as an alternative to paraffin-based ones, PCMs based on sugar alcohols have attracted much attention because of their superior performance in terms of both latent heat and thermal conductivity. The latent heat and thermal conductivity of sugar alcohol PCMs have been investigated in many experiments [10–12], which show that the thermal conductivity of most sugar alcohols, even pure materials without any additives or functional group modifications, is often higher than that of paraffin-based composite PCMs, which use various means to improve heat transfer properties. Therefore, sugar alcohols have a strong potential as a new generation of PCMs for commercial application in the future. Reflecting such interest, there has already been a large number of experimental and theoretical investigations of sugar alcohol in recent years [13]. Although compared to paraffin, sugar alcohols have better performance as PCMs due to larger latent heat, because of a high degree of supercooling, solidification frequently happens much below the freezing point, which is undesirable. To remedy this, nano-additives are often added to promote nucleation that would trigger solidification in sugar alcohols and reduce the supercooling tendencies, while also further enhancing the effective thermal conductivity [14,15]. As more intrinsic knowledge of the phase change mechanism in sugar alcohol PCMs will be obtained in this work, it is hoped that it also might eventually lead to better approaches to controlling this problem.

Several recent molecular dynamics studies on sugar alcohols have found that the melting of different crystalline surfaces happens at different temperatures [16,17]. It has been suggested that this is due to the varying strength of intermolecular forces in different lattice directions [18]. This anisotropic phenomenon was also observed in the surface melting of ice in earlier experiments [19]. However, the actual mechanism of this anisotropic melting phenomenon has not been investigated in detail, and it is believed that this anisotropic melting could have great potential for the future application of phase change materials, e.g. controlling phase change temperature of a single PCM type to satisfy diverse working conditions. On the other hand, because sugar alcohols have the same number of hydroxyl groups as their carbon atoms, their various physical properties are often strongly influenced by the complex and large number of hydrogen bonds in their crystalline states, which not only affects the phase transition process but also affects their latent heat and other physical properties [20]. It has been shown that the hydroxyl groups have an important influence on the physical properties of sugar alcohols, as isomers with the same molecular formula have been found to have different latent heat due to different hydroxyl positions [17]. In general, for paraffin PCMs, latent heat per mole (kJ/mol) has a proportional relation to the number of carbon atoms, but for sugar alcohol molecules, the amount of latent heat of sugar alcohols sometimes does not necessarily increase with an increase in the number of carbon atoms and hydroxyl groups, and the latent heat per mole of some short-chain sugar alcohols is known to even be larger than that of long-chain sugar alcohols, not to mention the latent heat per unit mass (kJ/kg) [21]. To the best of our knowledge, there have been no comparative studies on the latent heat of sugar alcohols with different numbers of carbon atoms to explain the causes of the latent heat difference between different sugar alcohols. The exploration of differences in the latent heat will reveal the key factors determining its magnitude and further deepen the understanding of sugar alcohol PCMs.

Therefore, in this study, four sugar alcohols: glycerol (C<sub>3</sub>H<sub>8</sub>O<sub>3</sub>), erythritol (C<sub>4</sub>H<sub>10</sub>O<sub>4</sub>), arabinitol (C<sub>5</sub>H<sub>12</sub>O<sub>5</sub>), and mannitol (C<sub>6</sub>H<sub>14</sub>O<sub>6</sub>), which contain three, four, five, and six carbon atoms, respectively, were chosen and the phase change properties such as melting point and latent heat were investigated via molecular dynamics simulations. The melting temperatures under different one-dimensional heat conduction

directions in relation to the crystal lattice were obtained. Anisotropic melting tendencies were found and investigated via the molecular orientation of the crystal state and intermolecular interactions. The latent heat of the four sugar alcohols was also calculated, and the detailed contributions to latent heat were decomposed into the contributions of various molecular interactions. Properties and behaviors of hydrogen bonds were analyzed as well to discuss the similarities and differences in the contributions.

## 2. Simulation details

### 2.1. Force fields and simulation setup

The OPLS-AA (all atom) force field [22–24] applied in this study has widely been used in many studies to investigate the properties of alcohols [25]. The potential energy terms in the OPLS-AA force field are as follows:

$$E_{\text{pot}} = E_{\text{bonds}} + E_{\text{angles}} + E_{\text{dihedrals}} + E_{\text{unbonded}} \quad (1)$$

$$E_{\text{bonds}} = \sum_{\text{bonds}} K(d - d_0)^2 \quad (2)$$

$$E_{\text{angles}} = \sum_{\text{angles}} k(\theta - \theta_0)^2 \quad (3)$$

$$E_{\text{dihedrals}} = \sum_{\text{dihedrals}} \frac{1}{2} \{ V_1[1 + \cos(\varphi)] + V_2[1 - \cos(2\varphi)] + V_3[1 + \cos(3\varphi)] + V_4[1 - \cos(4\varphi)] \} \quad (4)$$

$$E_{\text{unbonded}} = \sum_{i>j} \epsilon_{ij} \left( \frac{\sigma_{ij}}{r_{ij}^{12}} - \frac{\sigma_{ij}}{r_{ij}^6} \right) + \sum_{i>j} \left( \frac{q_i q_j}{4\pi\epsilon_0 r_{ij}} \right) \quad (5)$$

where the first three terms in Eq. (1) represent interatomic stretching, bending, and torsion energies.  $d$  is the distance between two bonding atoms,  $\theta$  is the angle between three bonding atoms,  $\varphi$  is the dihedral formed by four atoms,  $d_0$ ,  $\theta_0$  are the equilibrium bond length and angle,  $K$ ,  $k$ ,  $V$  are energy coefficients and subscripts  $i$  and  $j$  are atom indices. The last term  $E_{\text{unbonded}}$  in Eq. (5) consists of two parts that represent intermolecular interactions. The first part is the 12-6 Lennard-Jones potential, which we use to describe the van der Waals (vdW) interactions, where  $\epsilon$  and  $\sigma$  are the energy and distance parameters, respectively. The second part describes the Coulombic energy, and  $q$  is the charge of the atom. Detailed value of parameters described above can be found in section S5 in Supporting Information. Unbonded interactions are not considered for bonded atoms, often noted in literature as 1-2 interactions, and for atoms connected by an intermediate bonded atom, noted as 1-3 interactions. When atoms are bonded via two intermediate atoms (1-4 interactions), both vdW and Coulomb interactions are scaled to 0.5. The cut-off distance is 12 Å for both vdW and Coulombic short-range interactions. The long-range Coulomb interactions are calculated by the particle-particle particle-mesh method with an accuracy of  $1 \times 10^{-6}$  [26]. The implementation of the SHAKE algorithm [27] with an accuracy tolerance  $1 \times 10^{-4}$  and maximum 100 of iterations in our simulations ensures to avoid the quick vibration of the bonds connected to hydrogen atoms to reduce calculation complexity and speed up the simulation. Three-dimensional periodic boundary conditions are applied in all directions for all simulations, and the integration time step is set to 1 fs. The velocity Verlet time-stepping algorithm is used to update the atom motions [28]. To precisely indicate the phase change properties of sugar alcohols, the correct crystal structure of solid sugar alcohols is indispensable. The crystal configurations of sugar alcohols are constructed using experimental data obtained via X-ray diffraction technique [29–32]. All simulation calculations in this work were performed by a Large-scale Atomic/Molecular Massively Parallel Simulator

(LAMMPS) [33] and we used Visual Molecular Dynamics (VMD) [34] software to visualize the molecular model construction.

## 2.2. Local equilibrium non-equilibrium molecular dynamics simulations

The melting point is an essential physical quantity that needs to be obtained first to examine phase change. An easy and direct way to determine the melting point is to heat a solid system at a fixed heating rate under constant pressure, and then observe at which temperature the volume abruptly changes. On the other hand, this is prone to overestimating the melting point, so-called superheating, because it is difficult to break the energy barrier between the solid and liquid phases at the melting point in a short time scale. This often leads to the melting occurring at a temperature higher than the macroscopic melting point [35].

To avoid such problems in molecular simulation, solutions with multiple procedures to create the solid-liquid interface, such as the interface/NPT method and the interface/NVE method have been proposed [35]. In our work, an alternative and convenient approach is adopted to determine the melting point of sugar alcohols, called the local equilibrium non-equilibrium molecular dynamics (LE-NEMD) method [36]. In the LE-NEMD system, heat is conducted along a specific lattice direction due to the hot and cold heat baths, as shown in Fig. 1, which also creates a one-dimensional temperature gradient, resulting in a solid-liquid coexisting configuration. As solid and liquid phases co-exist, the solid-liquid energy barrier no longer causes an overestimation of the melting point.

The LE-NEMD approach consist of two steps. First, three elongated crystalized configurations along (100), (010), and (001) crystal lattice directions are built with 2880, 2304, 2160, and 2400 molecules for mannitol, arabinitol, erythritol, and glycerol, respectively, by replicating the crystal unit cell from the experimental data [29–32] (detailed information of unit cell is given in section S1 of Supporting Information). The same number of molecules of each sugar alcohol is adopted regardless of the crystal lattice direction. The systems are then relaxed for 3 ns via applying Nosé–Hoover [37] barostat and thermostat (NPT) at a pressure of 1 atm and temperatures of 250 K, 300 K, 350 K, and 350 K for glycerol, arabinitol, erythritol, and mannitol, respectively, which are significantly below their experimental melting points of 291 K, 393 K, 373 K, and 442K [11,12], to ensure the formation of a crystal state. This produces three stable elongated crystal configurations along the three lattice directions for each sugar alcohol. As a second step, using the last state of the relaxation, system-wide thermostats are removed, and the Nosé–Hoover barostat is performed to control the pressure along the direction of temperature gradient under 1 atm, where only the length of this direction is relaxed. In other words, the system only expands or shrinks along the heat conduction direction during the simulation. The heat source and heat sink are implemented via Langevin heat baths [38] located on one side of the system as shown in Fig. 1. The temperature of the heat sink is kept at the relaxation temperature, while that of the heat

source is set to 400 K, 450 K, 580 K, and 650 K for glycerol, arabinitol, erythritol, and mannitol, respectively. It is essential to mention that the temperature of the heat source is set to sufficiently higher than the experimental melting point to ensure that the hot side of the system is completely melted. After a 35 ns run, the systems become stable, and the solid-liquid interface is established stationarily, sampling data is collected from last 5 ns. Please note that because the position of the interface is not directly used in our work, the solid-liquid interface shown in Fig. 1 is a rough estimation. The determination method is introduced in section S6 in Supporting Information. In this stable state, a fixed temperature gradient forms along the heat flow direction, and in the right-hand side area of the system, which is the data sampling region of the system, as indicated in Fig. 1. Every yz slab of the region can be assumed to be in an equilibrium state since the temperature gradient of these sections is very small and invariant to time. Thus, the physical quantities such as temperature, energy and density in each small section can be independently calculated. From the sampling region of the LE-NEMD system, the temperature and the energy are both the function of position along the heat conduction direction, therefore the relation between the energy and temperature can be obtained. Because a solid-liquid interface exists, a total energy (kinetic and potential energy) jump occurs near its interface position, which can be reflected in the energy-temperature curve. To pinpoint the temperature of the phase change, the energy-temperature curve in the sampling area is fitted by a cubic spline and its derivative is taken, as shown in Fig. 2. The melting point can then be determined as the temperature at which the derivative has the maximum value, i.e., where the energy-temperature curve has the highest gradient, as shown as the red arrow in the smaller embedded graph of Fig. 2. In addition, the energy difference at the melting point

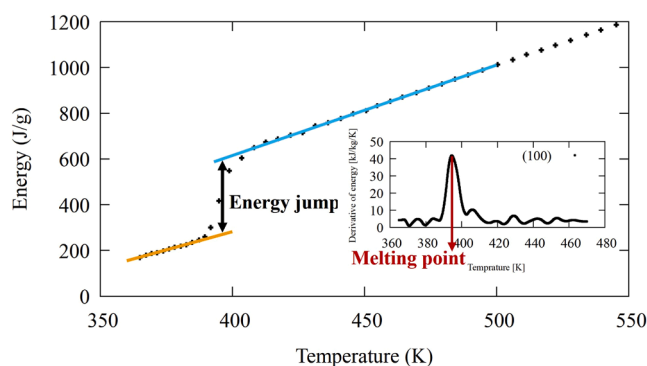


Fig. 2. An example of the latent heat and melting point calculation method in LE-NEMD simulations of erythritol (100) system. The blue and yellow lines are the linear extrapolations of the temperature-energy curve, and the energy jump represents a preliminary estimate of latent heat. The lower right window is the derivative of the temperature-energy curve, the red arrow points to the melting point.

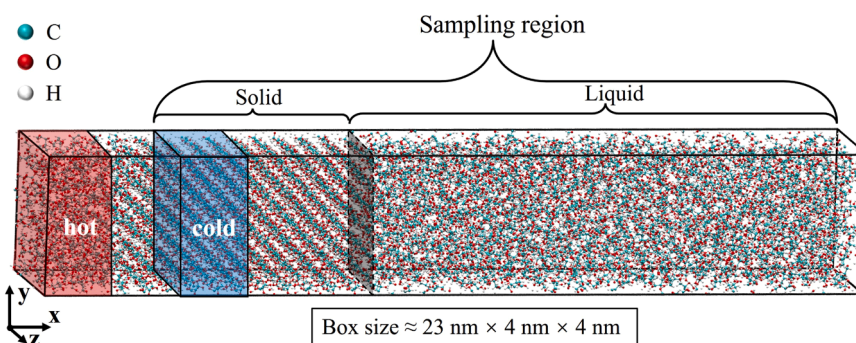


Fig. 1. Schematic of LE-NEMD system, erythritol (100) system given as an example, blue and red regions sign heat sink and heat source, gray plane indicates the rough position of the solid-liquid interface.

between the linear extrapolations of the temperature-energy curve from the solid and liquid sides can be used as a preliminary estimate of the latent heat of sugar alcohols (details can be found in section S2 of Supporting Information), as shown as the black bidirectional arrow in Fig. 2.

Because of the anisotropy of the crystal structures of sugar alcohols, the melting points obtained from LE-NEMD systems constructed along the (100), (010), and (001) directions have a non-negligible difference. As we are also interested in the bulk properties and want to determine the latent heat, which should not depend on the crystal direction, the bulk melting point is chosen as the lowest value, as melting in real materials is assumed to start from the easiest direction. Fig. 1 is one example configuration of the LE-NEMD system, where the molecules are aligned along with (100) direction.

### 2.3. Equilibrium bulk simulation

In principle, a rough estimation of the latent heat can be obtained together with the melting point from the LE-NEMD systems described in 2.1. After knowing melting point, to reduce the analysis complexity, a more robust and simpler method is used to determine the latent heat of fusion. First, two equilibrium bulk systems are constructed: one in a solid phase at the melting point, and the other in a liquid phase, also at the same melting point and pressure. The latent heat can be then derived as the enthalpy difference between the two phases [39], as shown in Eq. (6):

$$\begin{aligned} \Delta H_{\text{fusion}}(p, T) &= H_l(p, T) - H_s(p, T) \\ &= E_l^{\text{tot}}(p, T) - E_s^{\text{tot}}(p, T) + p(V_l(p, T) - V_s(p, T)), \end{aligned} \quad (6)$$

where the enthalpy of fusion  $\Delta H_{\text{fusion}}(p, T)$  is the difference in enthalpy between the liquid and solid phases at a certain pressure  $p$  and the melting point  $T$ , represented as  $H_l(p, T)$  and  $H_s(p, T)$ , respectively.  $E_l^{\text{tot}}(p, T)$  and  $E_s^{\text{tot}}(p, T)$  are the total energy of the liquid and solid phases; and  $V_l(p, T)$  and  $V_s(p, T)$  are the system volumes of liquid and solid phases, respectively. As the temperatures are the same, the solid and liquid phases have the same amount of kinetic energy; in addition, compared with vaporization, the volume change of the melting process can be considered negligible. Therefore, we can approximate that  $\Delta H_{\text{fusion}}(p, T)$  is the difference in the potential energy between the solid and liquid phases, as shown in Eq. (7):

$$\begin{aligned} \Delta H_{\text{fusion}}(T) &= E_l^{\text{pot}}(p, T) - E_s^{\text{pot}}(p, T) + p(V_l(p, T) - V_s(p, T)) \\ &\approx E_l^{\text{pot}}(p, T) - E_s^{\text{pot}}(p, T), \end{aligned} \quad (7)$$

As shown in Fig. 3 the initial configurations of the bulk systems are also built from the crystal unit cell [29–32]. In the case of liquid systems, the crystal lattice is first melted via annealing for 3 ns, under 1 atm and at 450 K, 600 K, 500K, and 650 K for glycerol, arabinitol, erythritol, and

mannitol, respectively, into a liquid phase, and then gradually cooled down to melting temperature under 2 ns at a fixed rate, while remaining in a liquid phase. Solid systems don't need annealing and are relaxed from their initial configuration. Bulk solid and liquid systems are both relaxed and sampled under an NPT ensemble under 1 atm at the melting point for 3 ns and 5 ns, respectively. Directional components of the system pressure are controlled independently for solids in the triclinic box and shear stress is not relaxed, i.e., system size can change in each direction independently, while they are coupled for liquids. The bulk systems consisted of 540, 512, 432, and 480 molecules for mannitol, arabinitol, erythritol, and glycerol, respectively. Three-dimensional periodic boundary conditions are applied to all the bulk systems. The systems are used to determine latent heat and its decomposition analysis in which governing factors and their contributions are evaluated. Additionally, hydrogen bond analysis and interaction energy analysis are carried out to further investigate the phase change properties of sugar alcohols.

## 3. Result and discussion

### 3.1. Melting point and latent heat

The LE-NEMD (100) system of erythritol is demonstrated in Fig. 4, where the profiles of temperature, density, and total energy at every slab are calculated. The energy-temperature curves of all four sugar alcohols are plotted in Fig. 5. The melting points are determined via the approach described in Section 2.1 for each lattice direction, with the results shown in Table 1, where experimental values are obtained from Refs. [11,12]. It is found that the melting point of mannitol in the (100) direction  $T_m^{C_6H_{14}O_6}(100) = 456$  K was lower than  $T_m^{C_6H_{14}O_6}(010) = 488$  K by approximately 32 K, and  $T_m^{C_6H_{14}O_6}(100)$  is lower than that of  $T_m^{C_6H_{14}O_6}(001) = 506$  K by approximately 19 K. This means that the energy jump, observed at the solid-liquid interface in Fig. 4, where the phase change occurs, happens at different temperatures under different directions of heat conduction even for the same material. In this work, we call this phenomenon as anisotropic melting. Similarly, this anisotropic melting tendency can also be found for arabinitol and glycerol, observed from the different temperature-energy curves in Fig. 5 as well. On the other hand, anisotropic tendencies were not apparent for erythritol. Please note that due to the arbitrariness of lattice direction definition, the relationship between temperature-energy curve and lattice directions of different sugar alcohols isn't rigidly defined. It is intrinsically affected by the molecular arrangement of sugar alcohol's own crystal structure alongside different lattice directions. This phenomenon is discussed in detail later in 3.2.

As mentioned in Section 2.2, the lowest computed melting temperature in Table 1 is considered as the macroscopic melting point of each sugar alcohol. Therefore, the macroscopic melting points of arabinitol and erythritol are set as  $T_m^{C_5H_{12}O_5} = 366$  K and  $T_m^{C_4H_{10}O_4} = 395$  K,

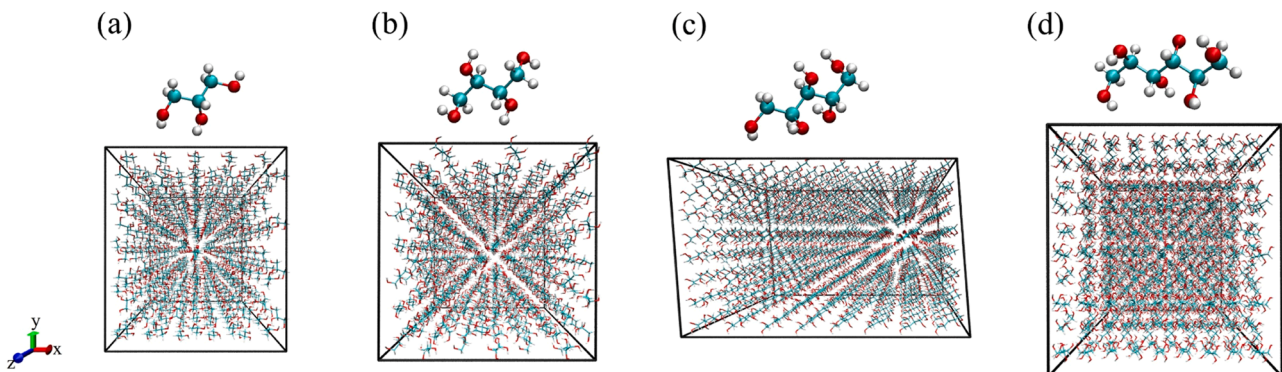


Fig. 3. Four sugar alcohol molecules and their bulk crystal configurations: (a) glycerol ( $C_3H_8O_3$ ), (b) erythritol ( $C_4H_{10}O_4$ ), (c) arabinitol ( $C_5H_{12}O_5$ ), (d) mannitol ( $C_6H_{14}O_6$ ).

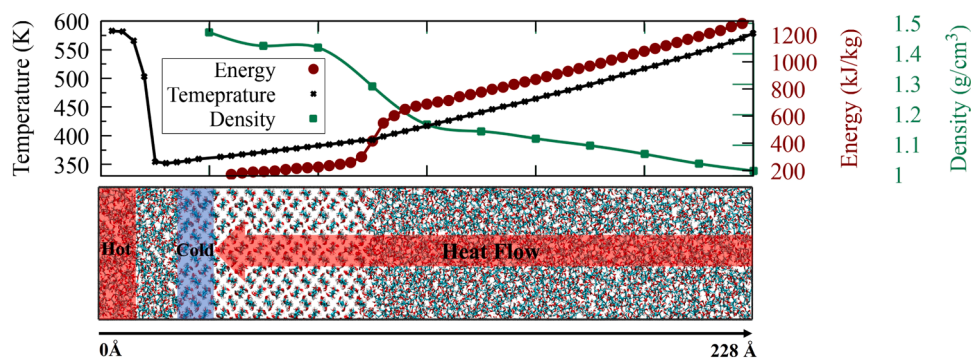


Fig. 4. LE-NEMD system of erythritol (100) direction and its energy, temperature, and density distribution along the heat conduction direction, respectively.

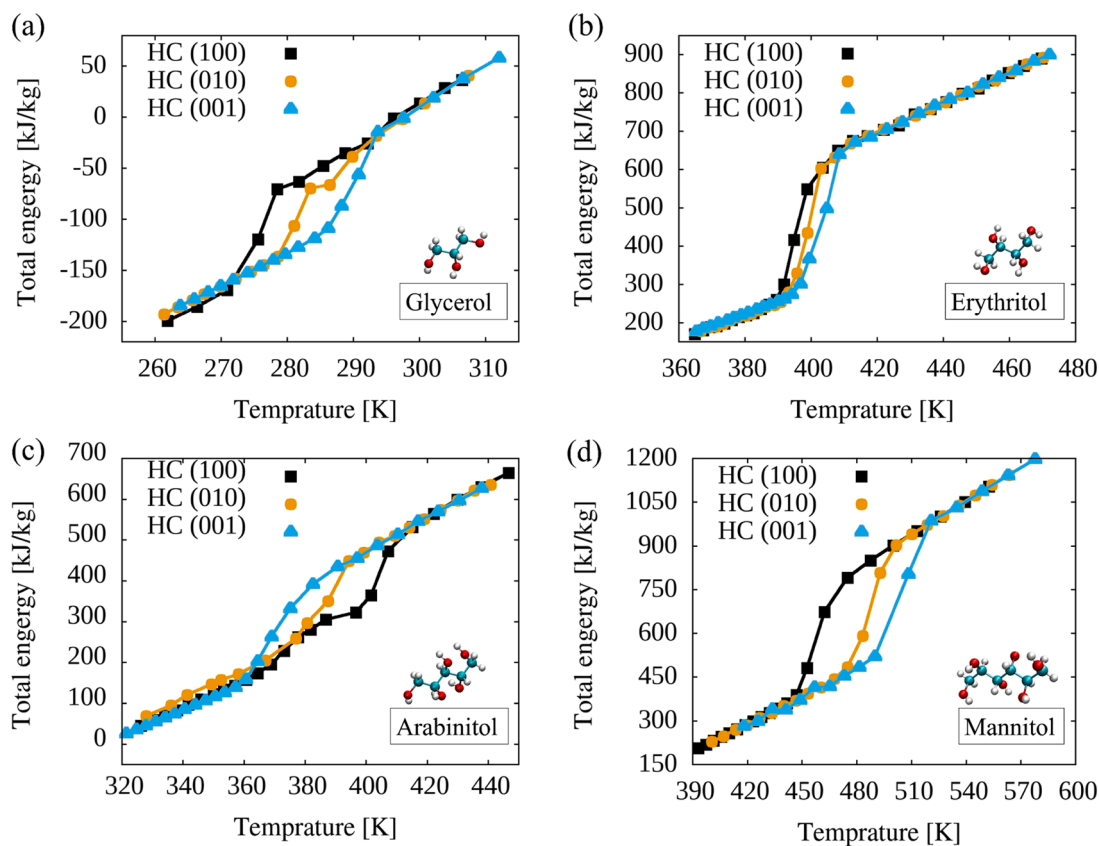


Fig. 5. Total energy as a function of temperature under different directions of heat conduction (HC): (a) glycerol, (b) erythritol, (c) arabinitol, (d) mannitol. Their derivative curves for melting point calculation are given in section S2 of Supporting information.

Table 1

Melting temperature (K) of sugar alcohols obtained via LE-NEMD simulations. Parentheses indicate standard errors (e.g.,  $276(2) = 276 \pm 2$ ).

Sugar alcohol	(100)	(010)	(001)	Expt. [11,12]
Glycerol	276(1)	282(2)	292(4)	291
Erythritol	395(3)	400(2)	406(8)	393
Arabinitol	404(1)	391(1)	366(4)	373
Mannitol	456(3)	488(2)	506(2)	442

respectively, which has a good agreement with experiment values of 373 K and 393 K. On the other hand, the melting point of mannitol, which is  $T_m^{C_6H_{12}O_6} = 456$  K, is somewhat larger than the experiment value of 442 K, while the melting point of glycerol  $T_m^{C_3H_8O_3} = 276$  K is smaller than the experimental value of 291 K, both having a deviation of more than 10 K.

Nonetheless, the observed experimental melting point trends of the four sugar alcohols, with mannitol having the highest melting point, and glycerol having the lowest, were properly reproduced via the solid-liquid coexistence LE-NEMD simulation, and the discrepancy between calculated and experiment values is less than 20 K.

As the melting points have been obtained for sugar alcohols, the liquid and solid phase bulk systems can now be constructed at these temperatures to measure latent heat, as described in 3.1. In brief, the latent heat of phase transition can be calculated according to Eq. (7) by obtaining the potential energy difference. The obtained latent heat of fusion for the four sugar alcohols is shown in Fig. 6. It is demonstrated that there is no simple correlation between the latent heat of the sugar alcohols and their chain length, as also observed in experiments. Erythritol with four carbon atoms and mannitol with six carbon atoms have similar latent heat values, which are much higher than that of arabinitol and glycerol with five and three carbon atoms, respectively.

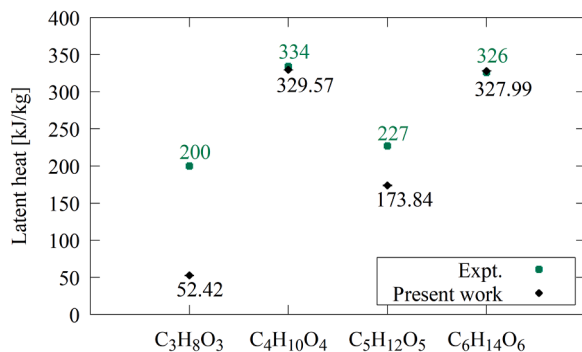


Fig. 6. Latent heat calculated via bulk simulations and experiment values [11, 12], note error bars of present work are very small as given by black hyphen marks.

On the other hand, in the case of glycerol, there is a large discrepancy between the present calculations and the experimental values, and it is suspected that some imperfectness of the OPLS-AA force field results in inadequate reproduction of intramolecular interactions of this sugar alcohol, which will be explained in 3.3. On the other hand, the obtained latent heat of fusion of all the other sugar alcohols is in good agreement with the experimental values, as indicated in Fig. 6, especially for erythritol and mannitol. Moreover, even considering the underestimation for glycerol, the relative magnitude relation of latent heat for the four sugar alcohols is in good agreement with the experimental results. Due to this, the simulation systems can be considered to reliably reflect the true phenomenon validating our MD analysis.

### 3.2. Mechanism of anisotropic melting tendencies

#### 3.2.1. Uniaxial order parameter

As demonstrated in Section 3.1, pronounced anisotropic melting tendencies are found in mannitol, arabinitol, and glycerol when the heat flow is applied along different lattice directions. It is known that because of the orientation of molecules that compose a crystal lattice, inherently anisotropic characteristics are prevalent in single crystals, i.e., for crystals without grain boundaries, the arrangement of molecules along different crystallographic directions is often different. In the LE-NEMD simulations in Section 3.1, the heat flow was along the three lattice directions of (100), (010), and (001), resulting in different alignments of the sugar alcohol molecules in relation to the heat flow. It is thought that such structural anisotropy translated into anisotropic melting. In order to characterize the arrangement of the molecules along a specific direction, the uniaxial order parameter [40] is used to measure the molecular arrangements along the three different heat flow directions. For a perfect molecular crystal, a single unit cell contains all the orientation information. Fig. 7 (a) shows the structure of the unit cell of arabinitol as an example. A carbon atom chain vector is defined as the displacement vector between the terminal carbons, with the angle between this vector and the direction of heat flow denoted as  $\theta$ . All the molecules in the unit cell are assigned an angle value  $\theta$ , and the uniaxial order parameter  $S_F$  can be calculated for each sugar alcohol along three heat flow directions via Eq. (8):

$$S_F = \left\langle \frac{3}{2} \cos^2 \theta - \frac{1}{2} \right\rangle. \quad (8)$$

where the subscript  $F$  in Eq. (8) represents the heat flow direction ((100), (010) or (001)), while the angle brackets denote a mean over all molecules in the unit cell. The uniaxial order parameter has a range of (-0.5,1) and indicates the orientation of the molecules in the unit cell. When the angles between the carbon atom chain vector and the heat flow direction are small, i.e., the molecules are mostly parallel to the heat flow direction, each value of the cosine is close to 1. In other words,

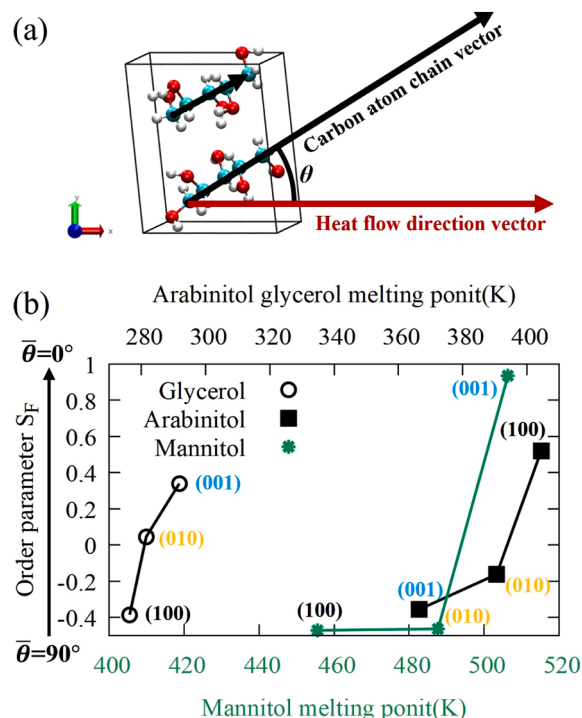


Fig. 7. (a) Unit cell of arabinitol, direction vectors and  $\theta$  definition. (b) uniaxial order parameter of sugar alcohols and its relationship to melting point.

if  $S_F$  is close to 1, most molecules are aligned parallel to the heat flow direction, while and if  $S_F$  is close to -0.5, most molecules are perpendicular to the heat flow direction. Fig. 7 (b) plots the relationship between the uniaxial order parameter  $S_F$  and the melting temperature in each direction of heat flow. It is found that the melting temperatures of arabinitol and glycerol tend to linearly increase with the increase of the order parameter. On the other hand, while  $S_{(100)}$  and  $S_{(010)}$  are similar for mannitol, the melting temperature is significantly different. It is thought to occur because the current order parameter definition only reflects the carbon chain orientation, while the orientation of hydroxyl groups may also greatly affect melting. In general, it is confirmed that there is a positive correlation between the order parameter and melting temperature, and that the direction with the higher melting temperature tends to have the larger order parameter. In other words, the more carbon atom chains of molecules align along the direction of heat flow, the higher melting temperature tends to be, the mechanism behind this will be introduced in 3.2.2 and 3.2.3. via means of analyses.

#### 3.2.2. Interaction energy

In 3.2.1, a correlation between the uniaxial order parameter and anisotropic melting tendencies was demonstrated. To investigate the mechanism, the bulk system introduced in Section 2.3 is used to carry out interaction energy analysis.

First, consider that melting is a process in which energy is absorbed by atoms or molecules in a crystal, and thermal fluctuation must reach a sufficient magnitude until it can break the energy barrier between the solid and liquid phases. For molecular crystals, it can be considered as a process where the constraints of the intermolecular forces are broken and thus the structure of the crystal is destroyed [18] so that molecules are able to move more freely. When the heat conduction is in one-dimension, similar to the LE-NEMD system in Fig. 4, but not at a stable state with progressive melting, at the solid-liquid interface, liquid molecules with higher energy gradually cause defects in the outermost layer of the crystal face (molecular layer) which transforms an ordered arrangement to a disordered state. For glycerol, arabinitol, and mannitol molecules, different directions of one-dimension heat conduction result

in different crystal faces that are crossed by the direction of heat flow are needed to break. Therefore, it is expected that the analysis of the interaction energy in relation to different crystal face structures may be able to reveal some relevant mechanisms. Among the three sugar alcohols with distinct anisotropic melting tendencies, arabinitol has the simplest triclinic crystal structure, as shown in Fig. 7(a), which makes it trivial to classify the different crystal faces and divide them into molecular layers. Fig. 8(a) shows a schematic diagram of the molecular layers division in the (100) direction (crystal unit cell extends in  $bc$  slab), along which crystalline arabinitol is divided into a total of 8 such molecular layers that have identical structure, where one of the molecular layers contains 64 molecules as indicated by a red box. The molecular layers in (010) and (001) directions which consist of the molecules in  $ac$  and  $ab$  slabs, respectively, are also treated in the same way and contain the same number of molecules as molecular layers (100). For these molecular layers, their intermolecular interactions (intermolecular potential energy of Eq. (5)) are divided into the interactions within the molecular layer, and the interactions with external molecules outside the layer, as respectively shown by the green and black arrows in Fig. 8(a). These two interactions are referred to as intralayer interactions and interlayer interactions, respectively. The intralayer and interlayer interaction energies for each condition are obtained from the mean of the 8 corresponding molecular layers. In order to observe the variation of these two interactions in the melting process of arabinitol, the temperature of this system is gradually increased from 300 K at the crystalline state to realize the melting process. The system finally reaches 550 K, which is a fully liquid state.

The magnitude and variation of intralayer and interlayer interaction energies of molecular layers of three directions in relation to temperature are shown in Fig. 8(b)–(c). The black, yellow, and blue dots indicate the interaction energies of the molecular layers in the (100), (010), and (001) directions, respectively, the negative energy values show attractive interactions. For this system, it is found that both the interaction energies of interlayer and intralayer start to show a sharp increase at around 400 K, where it is assumed that solid-liquid phase transition begins. It should be mentioned that for this kind of uniform heating system, the temperature required for the melting phase transition, i.e., melting point, is often overestimated due to the difficulty of breaking the solid-liquid energy barrier in a perfect solid crystal [41]. Nonetheless, it is possible to qualitatively assess the differences among different crystal faces. As mentioned earlier in this section, melting requires overcoming energy barriers between the solid and liquid states, and this should be reflected in the interaction energies of the molecular layers. As shown by the orange dotted line in Fig. 8(b)–(c), the interlayer interactions in Fig. 8(b) reach their maximum value at a lower temperature than the intralayer interactions in Fig. 8(c), which implies that the energy barriers of the interlayer interactions are easier to be overcome. On the other hand, more energy is needed to break the energy barriers of the intralayer interactions, which can be reflected by the amplitude of the energy jump that is defined as the energy difference between extremum value and the linear approximation of solid parts, as shown in Fig. 8(b)–(c). Therefore, it can be considered that the intralayer interaction plays a more critical role in the melting of one-dimensional heat conduction, as the key factor affecting the melting temperature. Intralayer energy

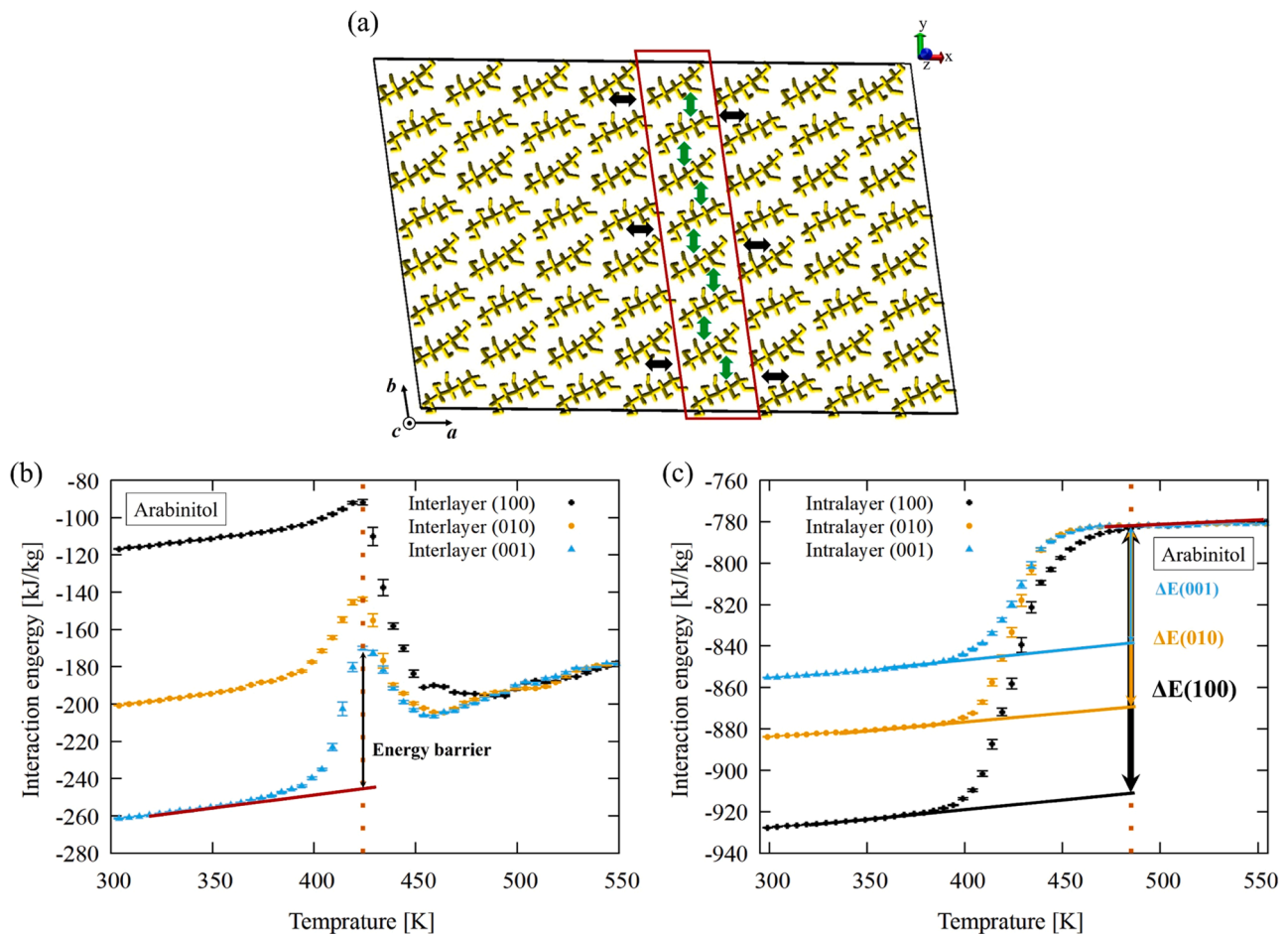


Fig. 8. (a) Schematic of interlayer and intralayer interactions of arabinitol, molecules are yellow for better visibility,  $a$ ,  $b$ , and  $c$  are three basic lattice directions and  $a \neq b \neq c$ , (b) arabinitol interlayer interaction energy in relation to temperature, (c) arabinitol intralayer interaction energy in relation to temperature, length of arrows  $\Delta E$  denotes energy barrier. For (b) and (c), dotted lines represent extremum of interaction energy.

barriers that need to be overcome to melt are shown in Fig. 8(c): the (100) molecular layer has the largest energy barrier, followed by (010), with (001) being the smallest. This is well correlated to the melting temperatures obtained by the LE-NEMD method in Table 1. Therefore, it is speculated that the energy barrier size that the molecular layer needs to overcome might directly determine anisotropic melting temperature tendencies that were observed in the case of one-dimensional heat conduction in 3.1. The same mechanism is possibly valid for other sugar alcohol molecules with anisotropic melting tendencies under different one-dimensional heat conduction, i.e., intralayer intermolecular interactions play an important role in the melting process. Moreover, it has been observed that interlayer interactions exhibit a decline after reaching their peaks as shown in Fig. 8(b). In our speculation, considering the intralayer interaction as the key factor affecting melting, the interlayer energy change appears to be a passive result due to the intralayer structure change, but the mechanism under this phenomenon haven't been fully understood.

### 3.2.3. Intralayer hydrogen bond

As it has been established that intermolecular energies play an important role in determining melting properties, attention is directed to hydrogen bonds. Arabinitol molecules have abundant hydroxyl groups, which are prone to forming hydrogen bonds with strong interactions. It is believed that the formation of hydrogen bonds is a good indication of the overall degree of intermolecular interactions. Therefore, the number of hydrogen bonds within the molecular layers of different orientations for arabinitol has been analyzed via the same bulk system used in 3.2.2 as well.

Fig. 9(a) shows the geometrical hydrogen bond definition adopted in this study, where the acceptor and donor oxygen cut-off distance is chosen as 3.5 Å. The cut-off distance was determined based on the radius distributional function (RDF) of oxygen atoms (see section S4 of Supporting Information). The cut-off angle was set to be 30° since the hydrogen bond would break if the amplitude of its librational movements surpasses 30° [42]. Fig. 9(b) shows an illustration of hydrogen bonding inside the molecular layer of three different orientations, and we can observe that the (100) molecular layer has a denser intralayer hydrogen bond network in comparison with the other two. The response of the number of hydrogen bonds to temperature is shown in Fig. 9(c). The hydrogen bond number inside the molecular layer in the (100) direction is always highest, followed by (010), and (001) in the temperature range of about 300–410 K, where the crystal structure is still present. At higher temperatures, the number of hydrogen bonds tends to become the same, as the system becomes liquid, and there is no longer memory of the initial layer configuration. The higher number of hydrogen bonds correlates with a larger intralayer potential energy barrier observed in Fig. 8(b) and a higher melting point indicated in Table 1. We can expect the crystal structure to be harder to break apart if it has a denser hydrogen bond network. This indicates that hydrogen bond information can be used as an important indicator of melting tendencies.

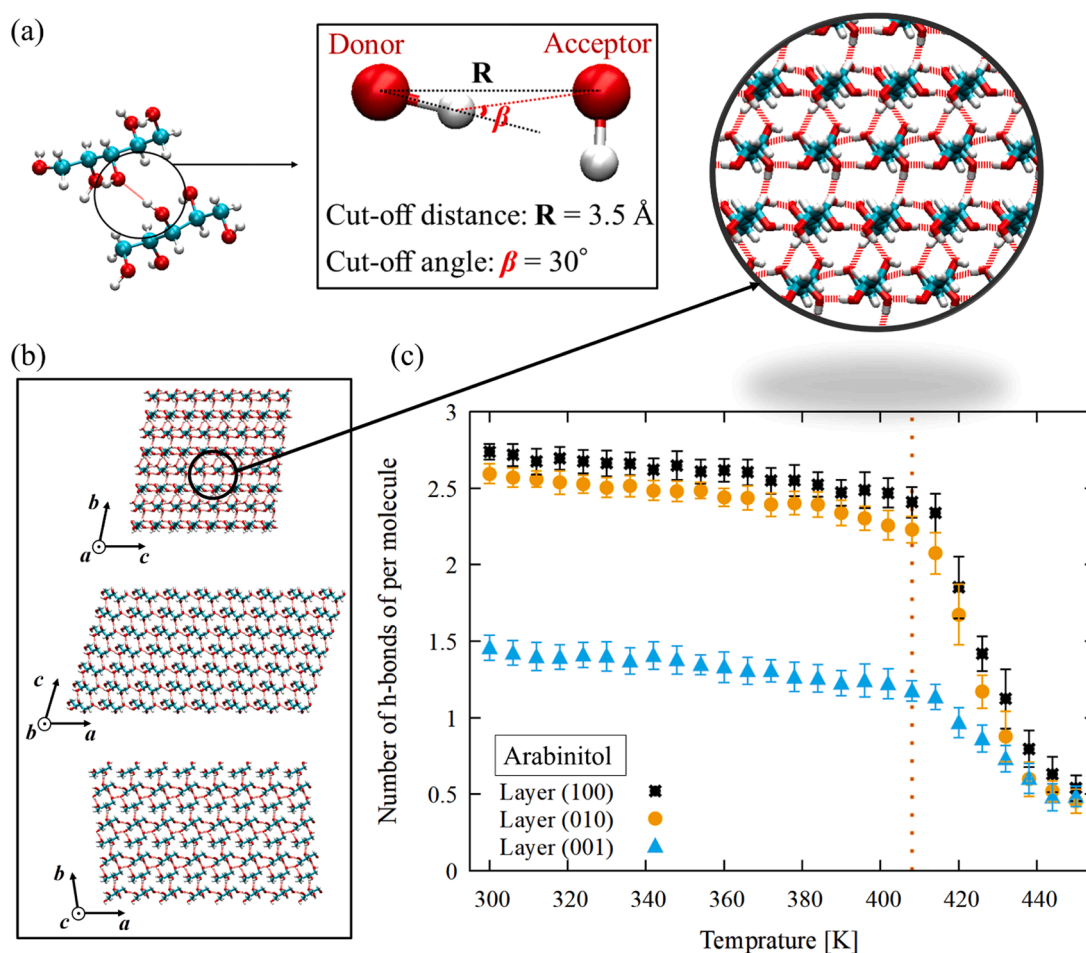


Fig. 9. (a) Geometrical hydrogen bond formation definition, (b) snapshot of hydrogen bonds of the arabinitol molecular layer (100), (010) and (001) from top to bottom, hydrogen bonds are indicated by red dashed lines as shown in the top right enlarged figure, (c) arabinitol per layer intralayer hydrogen bonds number in relation to temperature, dash line indicates the begin of melting in this bulk system.

### 3.3. Analysis of latent heat

#### 3.3.1. Decomposition of latent heat

To obtain a deeper understanding of the mechanism determining the latent heat, it is decomposed into contributing components for the equilibrium bulk systems. The latent heat of fusion of the sugar alcohols is divided into three main components according to their potential energy composition as described in Eq. (1): the intramolecular bonded component (bond, angle, and dihedral), the van der Waals (vdW) component, and the Coulombic component.

Latent heat decomposition result is shown in Fig. 10(a). We have found a significant underestimation of the latent heat only for glycerol, as mentioned in 3.1. Now it can be concluded that is due to the intramolecular bonded component that exhibits a large negative value which is very different from other alcohols in this work. A further examination reveals that the specific cause of this large negative bonded energy is due to a very large negative dihedral potential's contribution (see section S3 of Supporting Information). This is resulting from the fact that the OPLS-AA force field produces a high energy value in the dihedral potential at the crystalline state. It has been found in a study that the OPLS-AA force field has some deficiencies when describing glycerol [43]. It is believed that if the dihedral description can be improved, the latent heat assessment of glycerol would be closer to the experimental value. In addition, it is found that the intramolecular bonded component contributes negatively to the latent heat also in mannitol. That is because the molecules are in a regular arrangement in the crystalline state due to mutual constraints but in the liquid state the constraints are broken, leading to greater freedom. Energetically, for mannitol and glycerol, the liquid phase is more stable if only considering bonded interactions. On the other hand, the vdW and Coulomb components consistently contribute positively to the latent heat, and the magnitude of the contribution of those two unbonded components is always larger than that of the bonded component for all sugar alcohols. For example, in the

case of erythritol, the contribution of the van der Waals component and the Coulombic component is 258.90 kJ/kg, which is about 77% of the total latent heat 337.39 kJ/kg, demonstrating the substantial contribution of unbonded interactions.

To get an alternative perspective of latent heat composition, the unbonded components have been also decomposed by the interacting atom groups. Since sugar alcohols possess a large number of hydroxyl groups, atoms are divided into OH and CH<sub>n</sub> groups and contributions to latent heat due to OH–OH, CH<sub>n</sub>–CH<sub>n</sub> and OH–CH<sub>n</sub> interactions are computed. The decomposition is shown in Fig. 10 (b), where it is found that the CH<sub>n</sub>–CH<sub>n</sub> and OH–OH interactions both have positive contributions to latent heat, with OH–OH being the main contributor. On the other hand, the OH–CH<sub>n</sub> interaction contribution is negative. Since the steric hindrance in molecular structure, i.e., hydroxyl groups distribute in the outmost part of a sugar alcohol molecule, result in closer OH groups than CH<sub>n</sub> groups, which is also confirmed with RDF (see section S4 of Supporting Information) and explains the larger OH–OH contribution. Taking into account the abundant amount of hydroxyl groups in sugar alcohols and that OH–OH interactions are the biggest contributors to latent heat, hydrogen bond analysis may provide further insight into the mechanism of latent heat.

#### 3.3.2. Analysis of hydrogen bonds

The hydrogen bond network has a significant effect on the properties of materials due to hydrogen bonds having very strong interactions. The geometric hydrogen bond definition is given in Fig. 9(a), and the same equilibrium bulk simulation systems in Section 3.3.1 are used for hydrogen bond analysis.

The hydrogen bond number per molecule in the solid and liquid phases of the four sugar alcohols is displayed in Table 2. For all sugar alcohols, the solid phase tends to have more hydrogen bonds than the liquid phase, while the hydrogen number difference between two phase is similar among different molecules. In other words, it can reflect that there is about one hydrogen bond lost during melting. Therefore, it can be considered that latent heat is partly due to the energy that is needed to break the hydrogen bonds during phase change. The average hydrogen bond length in Table 2 is defined as the mean O–O distance. While there is no significant difference among different sugar alcohol types, the hydrogen bonds in solid are slightly shorter than that in liquid states, which can be interpreted as solid phase having stronger attractive interactions.

Strictly speaking, the hydrogen bond number and length are not enough to describe all characteristics of hydrogen bonding, as stability is also another important factor that will affect hydrogen bonding states. To investigate hydrogen bond differences that are not reflected in mean numbers and length, hydrogen bond lifetime was also investigated.

The hydrogen bond lifetime [44] was evaluated via the MDanalysis Python package [45–47]. Eq. (9) gives the expression of continuous hydrogen bond lifetime  $C(t)$ :

$$C(t) = \left\langle \frac{\sum h_{ij}(t_0)h_{ij}(t_0 + t)}{\sum h_{ij}(t_0)^2} \right\rangle \quad (9)$$

where  $h_{ij} = 1$  indicates the continuous presence of a hydrogen bond between atoms  $i$  and  $j$ .  $h_{ij} = 0$  denotes a lack of hydrogen bond and will remain at  $h_{ij} = 0$  even if the hydrogen bond is reestablished later. The

**Table 2**

Hydrogen bond number (per molecule) and length (Å) of sugar alcohols in solid and liquid state, left-side values are number, right-side values are length.

Sugar alcohols	Solid	Liquid
Glycerol	2.68, 2.81	1.89, 2.81
Erythritol	2.74, 2.82	1.72, 2.87
Arabinitol	3.39, 2.81	2.14, 2.85
Mannitol	2.84, 2.85	2.18, 2.89

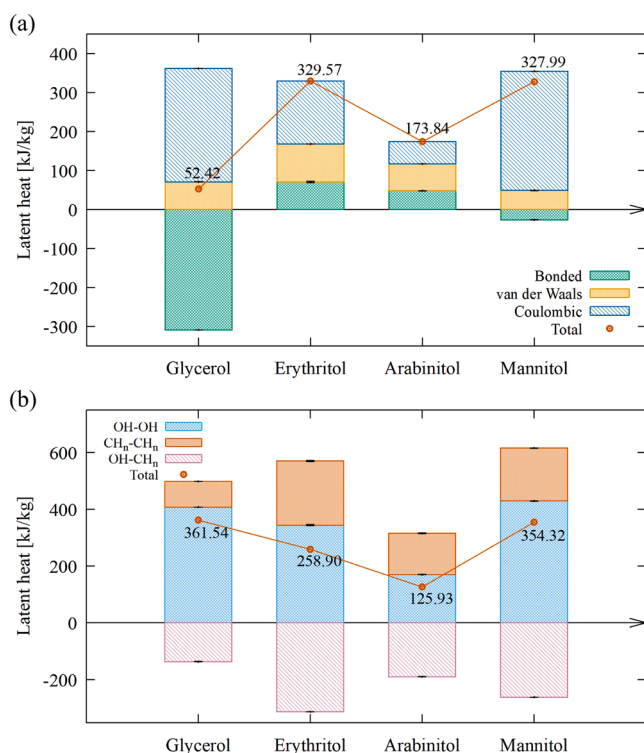


**Fig. 10.** (a) Latent heat decomposition into contributions from bonded, van der Waals, and Coulombic interactions, (b) unbonded components decomposition into contributions from CH and OH group interactions. Values represented by dots are the summations of all contributions.

summation is performed over all possible atoms, where all oxygen atoms are considered possible acceptors and donors. The angular brackets indicate an average over many different starting times in the trajectory.

Fig. 11 shows the hydrogen bond lifetime curve of four sugar alcohols in solid and liquid phases at the same temperature, respectively. It can be observed that hydrogen bond probability decreases to zero for all cases. This happens even in solids, because the strong vibration of hydroxyl groups at melting point would eventually causes temporary breakage of hydrogen bonds. Double exponential functions are used to fit the lifetime curve:

$$C(t) \approx A \cdot e^{-\frac{t}{\tau_1}} + B \cdot e^{-\frac{t}{\tau_2}} \quad (10)$$

where  $A$  and  $B$  represent the weight factors of the two exponentials, and  $\tau_1$  and  $\tau_2$  are the time constants. Double exponential functions have been used in previous literature [48,49] because of different decay scales of hydrogen bonds, which cannot be fully described by only a single exponential function. The overall lifetime can be obtained as  $\tau = A\tau_1 + B\tau_2$ . This overall lifetime can quantitatively explain the stability of hydrogen bonds, i.e., a larger lifetime would indicate stronger hydrogen bonds, which are harder to break. Hydrogen bond overall lifetimes are shown in Fig. 12. For all cases, hydrogen bond lifetime in solid phase is always larger than that in liquid phase, which indicates higher stability in solid. Furthermore, there appears to be some correlation between hydrogen bond lifetimes and latent heat of sugar alcohols. As indicated in Fig. 12 and Fig. 6, during melting, even number carbon atoms sugar alcohols, i.e., erythritol and mannitol whose hydrogen bond lifetimes are lower but have higher latent heat values which is counter-intuitive since longer hydrogen bond lifetimes usually reflect stronger interactions and should exhibit larger latent heat when they are broken. In

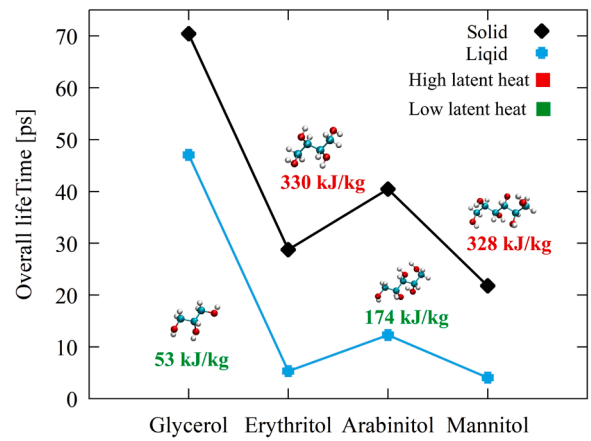


Fig. 12. Hydrogen bond lifetime constant of sugar alcohols and comparison with their latent heat.

our conjecture, in the melting process, if hydrogen bonding tends to be broken easily, what shows it is easy to absorb heat, may induce this material can have higher latent heat of fusion. But the reason behind this is still not very clear, the analysis here we adopted in this chapter is only particularly for hydrogen bonds since we speculated it contributes largely to latent heat. Besides hydrogen bonding, we think there may be other factors that can affect the latent heat of sugar alcohols, and further exploration will give a better expression.

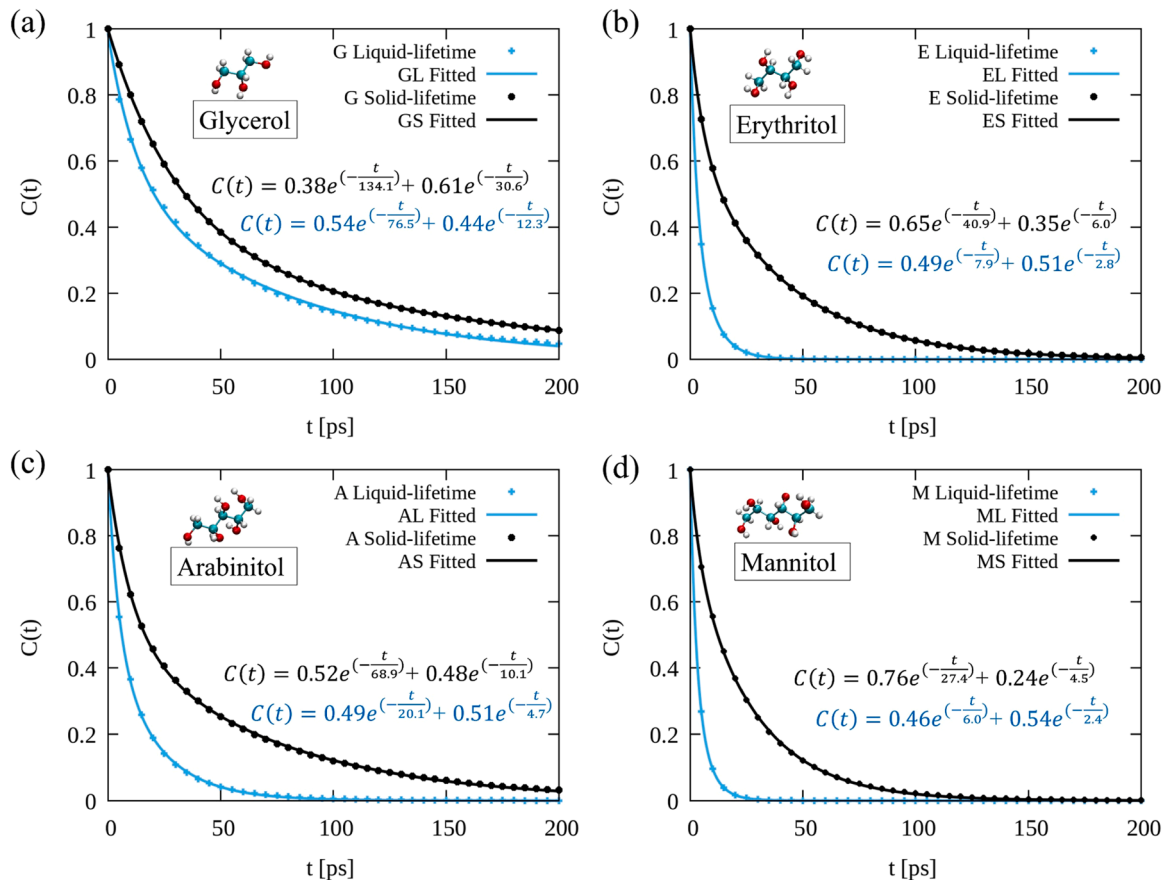


Fig. 11. Hydrogen bond lifetime curve with a fitted exponential function in the solid and liquid phases represented in black and blue, respectively, under the melting point temperature for (a) glycerol, (b) erythritol, (c) arabinitol, and (d) mannitol.

#### 4. Conclusions

In this study, the melting process and the latent heat of four sugar alcohols: glycerol (C<sub>3</sub>H<sub>8</sub>O<sub>3</sub>), erythritol (C<sub>4</sub>H<sub>10</sub>O<sub>4</sub>), arabinitol (C<sub>5</sub>H<sub>12</sub>O<sub>5</sub>), and mannitol (C<sub>6</sub>H<sub>14</sub>O<sub>6</sub>) have been investigated via molecular dynamics simulations.

By using a local-equilibrium non-equilibrium molecular dynamics (LE-NEMD) approach, the melting temperatures of the four sugar alcohols at 1 atm under the (100), (010), and (001) crystal lattice directions of one-dimensional heat conduction were calculated. Anisotropy of melting, i.e., different melting temperature depending on the crystal lattice direction was found. When the heat flow is applied along different sugar alcohol crystal lattice directions, the melting temperatures of mannitol, arabinitol, and glycerol are significantly different, i.e., anisotropic melting tendencies, correlated to molecular orientation were observed. To understand this phenomenon, the intermolecular interactions of molecular layers during the melting process of arabinitol crystal lattice were analyzed. It was found that the intralayer interactions have a more important influence on the anisotropic melting tendencies than the interlayer interactions. It appeared that larger energy barriers of intralayer interactions during phase change correlated to higher melting temperatures in each specific crystal lattice direction. This was also investigated via hydrogen bonding within the molecular layers, where a higher number of hydrogen bonds indicated stronger constraints within the molecular layer and are thought to lead to higher melting temperatures.

The latent heat of fusion of sugar alcohols was calculated and a good agreement with the experimental trends was observed. To reveal the mechanism of the latent heat, the latent heat has been decomposed into separate contributions based on atomic interactions. Unbonded interactions, composed of van der Waals (vdW), and Coulombic energies made up the largest contributions to latent heat. It was found that because the numerous hydroxyl groups in sugar alcohols are in close proximity to each other, a large portion of the contribution to latent heat comes from the interaction between hydroxy groups. Specifically, it was found that the number of hydrogen bonds decreases during melting, indicating that hydrogen bond breakage has a large effect on latent heat. There was also a correlation, where sugar alcohols with an even number of carbon atoms and the shorter hydrogen bond lifetimes had larger latent heat values. It is expected that sugar alcohols with higher positive vdW and Coulombic contribution to the latent heat tend to have higher latent heat and are therefore considered better candidates for phase change materials.

These results contribute to the innovative design of phase change materials based on sugar alcohols and give us a better understanding of their phase change mechanisms.

#### CRedit authorship contribution statement

**Shukai Cheng:** Writing – review & editing, Writing – original draft, Visualization, Software, Methodology, Investigation, Data curation, Conceptualization. **Donatas Surblys:** Writing – review & editing, Software, Methodology, Conceptualization. **Taku Ohara:** Writing – review & editing, Project administration, Conceptualization.

#### Declaration of competing interest

The authors declare that they have no known competing financial interests or personal relationships that could have appeared to influence the work reported in this paper.

#### Data availability

Data will be made available on request.

#### Acknowledgment

A part of this work was supported by JSPS KAKENHI JP24K00815. All the computational simulations were performed on the Supercomputer system “AFI-NITY” at the Advanced Fluid Information Research Center, Institute of Fluid Science, Tohoku University.

#### Supplementary materials

Supplementary material associated with this article can be found, in the online version, at [doi:10.1016/j.ijheatmasstransfer.2024.126104](https://doi.org/10.1016/j.ijheatmasstransfer.2024.126104).

#### References

- [1] A. Ribezzo, G. Falciani, L. Bergamasco, M. Fasano, E. Chiavazzo, An overview on the use of additives and preparation procedure in phase change materials for thermal energy storage with a focus on long term applications, *J. Energy Storage* 53 (2022) 105140, <https://doi.org/10.1016/j.est.2022.105140>.
- [2] M. Pomianowski, P. Heiselberg, Y. Zhang, Review of thermal energy storage technologies based on PCM application in buildings, *Energy Build.* 67 (2013) 56–69, <https://doi.org/10.1016/j.enbuild.2013.08.006>.
- [3] F. Souayfane, F. Fardoun, P.H. Biwole, Phase change materials (PCM) for cooling applications in buildings: a review, *Energy Build.* 129 (2016) 396–431, <https://doi.org/10.1016/j.enbuild.2016.04.006>.
- [4] Y. Zhou, F. Liu, H. Wang, Novel organic–inorganic composites with high thermal conductivity for electronic packaging applications: a key issue review, *Polym. Compos.* 38 (2017) 803–813, <https://doi.org/10.1002/pc.23641>.
- [5] H. Tafrihi, S. Sadeghzadeh, R. Ahmadi, Molecular dynamics simulations of phase change materials for thermal energy storage: a review, *RSC Adv.* 12 (2022) 14776–14807, <https://doi.org/10.1039/D2RA02183H>.
- [6] R.K. Sharma, P. Ganesan, V.V. Tyagi, H.S.C. Metselaar, S.C. Sandaran, Developments in organic solid–liquid phase change materials and their applications in thermal energy storage, *Energy Convers. Manage.* 95 (2015) 193–228, <https://doi.org/10.1016/j.enconman.2015.01.084>.
- [7] C.Y. Zhao, Y.B. Tao, Y.S. Yu, Molecular dynamics simulation of nanoparticle effect on melting enthalpy of paraffin phase change material, *Int. J. Heat Mass Transf.* 150 (2020) 119382, <https://doi.org/10.1016/j.ijheatmasstransfer.2020.119382>.
- [8] H. Sun, D. Surblys, H. Matsubara, T. Ohara, Molecular dynamics study on the role of hydrogen bonds and interfacial heat transfer between diverse silica surfaces and organic liquids, *Int. J. Heat Mass Transf.* 208 (2023) 124091, <https://doi.org/10.1016/j.ijheatmasstransfer.2023.124091>.
- [9] H. Babaei, P. Keblinski, J.M. Khodadadi, Thermal conductivity enhancement of paraffins by increasing the alignment of molecules through adding CNT/graphene, *Int. J. Heat Mass Transf.* 58 (2013) 209–216, <https://doi.org/10.1016/j.ijheatmasstransfer.2012.11.013>.
- [10] A. Seppälä, K. Turunen, M.R. Yazdani, Thermal conductivity of sugar alcohols, *Sol. Energy Mater. Sol. Cells* 243 (2022) 111796, <https://doi.org/10.1016/j.solmat.2022.111796>.
- [11] E.P. del Barrio, A. Godin, M. Duquesne, J. Daranlot, J. Jolly, W. Alshaeer, T. Kouadio, A. Sommier, Characterization of different sugar alcohols as phase change materials for thermal energy storage applications, *Sol. Energy Mater. Sol. Cells* 159 (2017) 560–569, <https://doi.org/10.1016/j.solmat.2016.10.009>.
- [12] E. Palomo Del Barrio, R. Cadoret, J. Daranlot, F. Achchaq, New sugar alcohols mixtures for long-term thermal energy storage applications at temperatures between 70°C and 100°C, *Sol. Energy Mater. Sol. Cells* 155 (2016) 454–468, <https://doi.org/10.1016/j.solmat.2016.06.048>.
- [13] C. Liu, Q. Cheng, B. Li, X. Liu, Z. Rao, Recent advances of sugar alcohols phase change materials for thermal energy storage, *Renew. Sustain. Energy Rev.* 188 (2023) 113805, <https://doi.org/10.1016/j.rser.2023.113805>.
- [14] X. Li, J. Zhang, Y. Liu, Y. Xu, K. Cui, Z. Yao, B. Fu, C. Song, W. Shang, P. Tao, T. Deng, Supercooled sugar alcohols stabilized by alkali hydroxides for long-term room-temperature phase change solar-thermal energy storage, *Chem. Eng. J.* 452 (2023) 139328, <https://doi.org/10.1016/j.cej.2022.139328>.
- [15] X. Yan, H. Zhao, Y. Feng, L. Qiu, L. Lin, X. Zhang, T. Ohara, Excellent heat transfer and phase transformation performance of erythritol/graphene composite phase change materials, *Compos. Part B Eng.* 228 (2022) 109435, <https://doi.org/10.1016/j.compositesb.2021.109435>.
- [16] B. Feng, L.-W. Fan, Y. Zeng, J.-Y. Ding, X.-F. Shao, Atomistic insights into the effects of hydrogen bonds on the melting process and heat conduction of erythritol as a promising latent heat storage material, *Int. J. Therm. Sci.* 146 (2019) 106103, <https://doi.org/10.1016/j.ijthermalsci.2019.106103>.
- [17] T. Inagaki, T. Ishida, Computational analysis of sugar alcohols as phase-change material: insight into the molecular mechanism of thermal energy storage, *J. Phys. Chem. C* 120 (2016) 7903–7915, <https://doi.org/10.1021/acs.jpcc.5b11999>.
- [18] N. Mathew, T.D. Sewell, D.L. Thompson, Anisotropy in surface-initiated melting of the triclinic molecular crystal 1,3,5-triamino-2,4,6-trinitrobenzene: a molecular dynamics study, *J. Chem. Phys.* 143 (2015) 094706, <https://doi.org/10.1063/1.4929806>.
- [19] Y. Furukawa, H. Nada, Anisotropic surface melting of an ice crystal and its relationship to growth forms, *J. Phys. Chem. B* 101 (1997) 6167–6170, <https://doi.org/10.1021/jp9631700>.

- [20] T. Steiner, The hydrogen bond in the solid state, *Angew. Chem. Int. Ed.* 41 (2002) 48–76, [https://doi.org/10.1002/1521-3773\(200210\)41:1<48::AID-ANIE48>3.0.CO;2-U](https://doi.org/10.1002/1521-3773(200210)41:1<48::AID-ANIE48>3.0.CO;2-U).
- [21] S. Tomassetti, A. Aquilanti, P.F. Muciaccia, G. Coccia, C. Mankel, E.A.B. Koenders, G. Di Nicola, A review on thermophysical properties and thermal stability of sugar alcohols as phase change materials, *J. Energy Storage* 55 (2022) 105456, <https://doi.org/10.1016/j.est.2022.105456>.
- [22] L.S. Dodda, J.Z. Vilseck, J. Tirado-Rives, W.L. Jorgensen, 1.14\*CM1A-LBCC: localized bond-charge corrected CM1A charges for condensed-phase simulations, *J. Phys. Chem. B* 121 (2017) 3864–3870, <https://doi.org/10.1021/acs.jpcc.7b00272>.
- [23] L.S. Dodda, I. Cabeza de Vaca, J. Tirado-Rives, W.L. Jorgensen, LigParGen web server: an automatic OPLS-AA parameter generator for organic ligands, *Nucl. Acids Res.* 45 (2017) W331–W336, <https://doi.org/10.1093/nar/gkx312>.
- [24] W.L. Jorgensen, J. Tirado-Rives, Potential energy functions for atomic-level simulations of water and organic and biomolecular systems, *Proc. Natl. Acad. Sci.* 102 (2005) 6665–6670, <https://doi.org/10.1073/pnas.0408037102>.
- [25] R. Zangi, Refinement of the OPLSAA force-field for liquid alcohols, *ACS Omega* 3 (2018) 18089–18099, <https://doi.org/10.1021/acsomega.8b03132>.
- [26] R.W. Hockney, J.W. Eastwood, *Computer Simulation Using Particles*, CRC Press, Boca Raton, 2021. <https://doi.org/10.1201/9780367806934>.
- [27] H.C. Andersen, Rattle: a “velocity” version of the shake algorithm for molecular dynamics calculations, *J. Comput. Phys.* 52 (1983) 24–34, [https://doi.org/10.1016/0021-9991\(83\)90014-1](https://doi.org/10.1016/0021-9991(83)90014-1).
- [28] L. Verlet, Computer “Experiments” on classical fluids. I. Thermodynamical properties of Lennard-Jones molecules, *Phys. Rev.* 159 (1967) 98–103, <https://doi.org/10.1103/PhysRev.159.98>.
- [29] J. Wouters, L. Van Meervelt, Classroom experiments with artificial sweeteners: growing single crystals and simple calorimetry, *Acta Crystallogr. Sect. E Crystallogr. Commun.* 78 (2022) 874–879, <https://doi.org/10.1107/S2056989022007617>.
- [30] T. Kusukawa, G. Niwa, T. Sasaki, R. Oosawa, W. Himeno, M. Kato, Observation of a hydrogen-bonded 3D structure of crystalline glycerol, *Bull. Chem. Soc. Jpn.* 86 (2013) 351–353, <https://doi.org/10.1246/bcsj.20120300>.
- [31] P. Derollez, Y. Guinet, F. Affouard, F. Danède, L. Carpentier, A. Hédoux, Structure determination of l-arabinol by powder X-ray diffraction, *Acta Crystallogr. B* 68 (2012) 407–411, <https://doi.org/10.1107/S0108768112019994>.
- [32] F.R. Fronczek, H.N. Kamel, M. Slattery, Three polymorphs ( $\alpha$ ,  $\beta$ , and  $\delta$ ) of d-mannitol at 100 K, *Acta Crystallogr. C* 59 (2003) o567–o570, <https://doi.org/10.1107/S0108270103018961>.
- [33] A.P. Thompson, H.M. Aktulga, R. Berger, D.S. Bolintineanu, W.M. Brown, P. S. Crozier, P.J. in ’t Veld, A. Kohlmeyer, S.G. Moore, T.D. Nguyen, R. Shan, M. J. Stevens, J. Tranchida, C. Trott, S.J. Plimpton, LAMMPS - a flexible simulation tool for particle-based materials modeling at the atomic, meso, and continuum scales, *Comput. Phys. Commun.* 271 (2022) 108171, <https://doi.org/10.1016/j.cpc.2021.108171>.
- [34] W. Humphrey, A. Dalke, K. Schulten, VMD: visual molecular dynamics, *J. Mol. Graph.* 14 (1996) 33–38, [https://doi.org/10.1016/0263-7855\(96\)00018-5](https://doi.org/10.1016/0263-7855(96)00018-5).
- [35] Y. Zhang, E.J. Maginn, A comparison of methods for melting point calculation using molecular dynamics simulations, *J. Chem. Phys.* 136 (2012) 144116, <https://doi.org/10.1063/1.3702587>.
- [36] H. Matsubara, T. Ohara, Effect of the in-plane aspect ratio of a graphene filler on anisotropic heat conduction in paraffin/graphene composites, *Phys. Chem. Chem. Phys.* 23 (2021) 12082–12092, <https://doi.org/10.1039/D1CP00556A>.
- [37] W.G. Hoover, Canonical dynamics: equilibrium phase-space distributions, *Phys. Rev. A* 31 (1985) 1695–1697, <https://doi.org/10.1103/PhysRevA.31.1695>.
- [38] R.L. Davidchack, R. Handel, M.V. Tretyakov, Langevin thermostat for rigid body dynamics, *J. Chem. Phys.* 130 (2009) 234101, <https://doi.org/10.1063/1.3149788>.
- [39] J. Wang, T. Hou, Application of molecular dynamics simulations in molecular property prediction. 1. Density and heat of vaporization, *J. Chem. Theory Comput.* 7 (2011) 2151–2165, <https://doi.org/10.1021/ct200142z>.
- [40] M.R. Wilson, Determination of order parameters in realistic atom-based models of liquid crystal systems, *J. Mol. Liq.* 68 (1996) 23–31, [https://doi.org/10.1016/0167-7322\(95\)00918-3](https://doi.org/10.1016/0167-7322(95)00918-3).
- [41] S.-N. Luo, T.J. Ahrens, T. Çağın, A. Strachan, W.A. Goddard, D.C. Swift, Maximum superheating and undercooling: systematics, molecular dynamics simulations, and dynamic experiments, *Phys. Rev. B* 68 (2003) 134206, <https://doi.org/10.1103/PhysRevB.68.134206>.
- [42] J. Teixeira, M.C. Bellissent-Funel, Dynamics of water studied by neutron scattering, *J. Phys. Condens. Matter* 2 (1990) SA105, <https://doi.org/10.1088/0953-8984/2/S/011>.
- [43] X. Dou, Y. Chen, Y. Han, Modification of glycerol force field for simulating silver nucleation under a diffusion limited condition, *Colloids Surf. Physicochem. Eng. Asp.* 592 (2020) 124574, <https://doi.org/10.1016/j.colsurfa.2020.124574>.
- [44] R.J. Gowers, P. Carbone, A multiscale approach to model hydrogen bonding: the case of polyamide, *J. Chem. Phys.* 142 (2015) 224907, <https://doi.org/10.1063/1.4922445>.
- [45] R.J. Gowers, M. Linke, J. Barnoud, T.J.E. Reddy, M.N. Melo, S.L. Seyler, J. Domański, D.L. Dotson, S. Buchoux, I.M. Kenney, O. Beckstein, MDAnalysis: a python package for the rapid analysis of molecular dynamics simulations, *Proc. 15th Python Sci. Conf.* (2016) 98–105. <https://doi.org/10.25080/Majara-629e541a-00e>.
- [46] N. Michaud-Agrawal, E.J. Denning, T.B. Woolf, O. Beckstein, MDAnalysis: a toolkit for the analysis of molecular dynamics simulations, *J. Comput. Chem.* 32 (2011) 2319–2327, <https://doi.org/10.1002/jcc.21787>.
- [47] P. Smith, R.M. Ziolk, E. Gazzarrini, D.M. Owen, C.D. Lorenz, On the interaction of hyaluronic acid with synovial fluid lipid membranes, *Phys. Chem. Chem. Phys.* 21 (2019) 9845–9857, <https://doi.org/10.1039/C9CP01532A>.
- [48] S. Bandyopadhyay, S. Chakraborty, S. Balasubramanian, B. Bagchi, Sensitivity of polar solvation dynamics to the secondary structures of aqueous proteins and the role of surface exposure of the probe, *J. Am. Chem. Soc.* 127 (2005) 4071–4075, <https://doi.org/10.1021/ja042847r>.
- [49] S. Bandyopadhyay, S. Chakraborty, B. Bagchi, Secondary structure sensitivity of hydrogen bond lifetime dynamics in the protein hydration layer, *J. Am. Chem. Soc.* 127 (2005) 16660–16667, <https://doi.org/10.1021/ja054462u>.